CrystEngComm

Accepted Manuscript

ROYAL SOCIETY OF CHEMISTRY

www.rsc.org/crystengcomm

CrystEngComm

RSCPublishing

COMMUNICATION

Layered photocatalyst $Bi_2O_2[BO_2(OH)]$ with internal polar field enhanced photocatalytic activity

Cite this: DOI: 10.1039/x0xx00000x

Rui Zhang,[a,b] Ying Dai,*[b] Zaizhu Lou,[a] Zhujie Li,[b] Zeyan Wang,[a] Yanmei Yang,[a] Xiaoyan Qin,[a] Xiaoyang Zhang[a] and Baibiao Huang*[a]

Received 00th January 2014,
Accepted 00th January 2014

DOI: 10.1039/x0xx00000x

www.rsc.org/

$Bi_2O_2[BO_2(OH)]$ nanosheets having an internal polar electric field in crystal structure are synthesized by one-step hydrothermal method. Due to the existence of internal polar electric field, the separation of photo-induced carriers can be enhanced, resulting in the high photocatalytic activity of $Bi_2O_2[BO_2(OH)]$ nanosheets under irradiation of UV light.

Since TiO_2 was firstly reported by Honda *et al* to have photocatalytic activity in hydrogen evolution, the semiconductor photocatalysis had been found to have important applications in energy and environment.[1] Various materials including Ag-based, Bi-based and solid solution materials were found to have photocatalytic activity under illumination of UV/Vis light.[2-4] In these materials, Bi-based materials have drawn much more attention for their unique layered crystal structures. For example, BiOX(X=Cl, Br, I), Bi_2WO_6 and $Bi_2O_2CO_3$ have layered structures which can result in different reaction sites for oxidization and reduction in the surface and edge of the 2D-layered structure, respectively.[5-6] However, their practical applications are still limited by the low quantum yield due to the rapid recombination of photo-generated carriers.[7-8] Some methods have been explored to enhance the separation of photo-generated electron-hole (e-h) pairs, such as composited photocatalysts, modification of noble metals and so on.[9-11] In these materials, photo-induced carriers can be separated by a field which is only existed in the interfaces of two materials, and the efficiency of charge separation is still low. Thus, to construct an internal electronic field in crystal structures of photocatalysts would be an efficient way to improve the charge separation for high quantum yield, sharply. [12]

Internal polar electric field has been verified to have an improvement role on the charge separation in $BiOIO_3$ which has an internal polar field constructed by the IO_3 pyramids to enhance the photocatalytic activity in photo-degradation of MO.[13] Because the constructed internal electric field needs to have the same direction with that of charge transfer, and few other materials with internal electronic fields are reported to have enhanced photocatalytic acitivity. So, construction of internal electric field along the direction of charge transfer is still a challenge. Recently, $Bi_2O_2[BO_2(OH)]$ was reported to have $BO_2(OH)$ pyramids,[14] and we have proved this structure owned an irresistible local dipole moments (Fig. 1). As a result, an internal polar field could be constructed by the ordered arrangement of $BO_2(OH)$ pyramids which has not been investigated (Fig. 1B). So, the study of internal polar field and its influence on photocatalytic activity of $Bi_2O_2[BO_2(OH)]$ is very significant.

Herein, $Bi_2O_2[BO_2(OH)]$ nanosheets were synthesized via a one-step hydrothermal method using polyvinylpyrrolidone (PVP) as a surfactant. With the ordered arrangement of $BO_2(OH)$ pyramids in single crystal sheets, an internal polar field is formed by the net dipole moment of $BO_2(OH)$ which is verified by the theoretical calculation. Photo-induced charges could transfer along opposite directions in the electric field, resulting in the high photocatalytic efficiency of $Bi_2O_2[BO_2(OH)]$ under UV light irradiation.

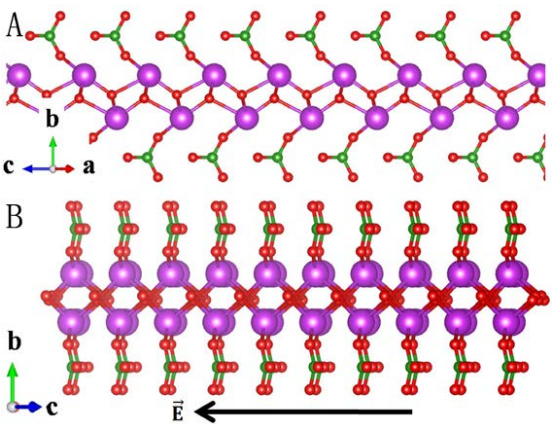

Fig. 1 A) A perspective view of Bi_2O_2 layer in $Bi_2O_2[BO_2(OH)]$, B) A perspective view of $Bi_2O_2[BO_2(OH)]$, in which shows the orientation of its internal polar field. (In the figure, the big purple circles represent Bi atoms, the small red and green circles represent O and B atoms, respectively.)

In order to confirm the ordered arrangement of $BO_2(OH)$ pyramids in crystal structure, $Bi_2O_2[BO_2(OH)]$ single crystal nanosheets were synthesized by using $Bi(NO_3)_3{\cdot}5H_2O$ and H_3BO_3 during a hydrothermal process. SEM images and XRD patterns of samples

prepared at 120 °C for different reaction time were shown in Fig. 2. At 3 h, precursor plates with a large size are the main products and $Bi_2O_2[BO_2(OH)]$ begins to form on the surface of precursor, which can be confirmed by SEM image (Fig. 2A) and XRD patterns

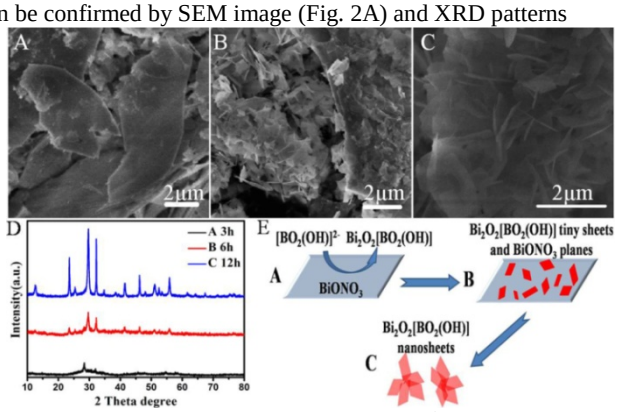

Fig. 2 SEM images (A-C) and XRD patterns (D) of samples prepared with 0.027 mM $Bi(NO_3)_3 \cdot 5H_2O$, 0.216 M H_3BO_3 and 0.0133 mM PVP at 120 °C for different reaction time : 3 h (A), 6 h (B) and 12 h (C); E) growth mechanism of $Bi_2O_2[BO_2(OH)]$ nanosheets.

(Fig. 2D(A)). As the reaction time prolongs, $Bi_2O_2[BO_2(OH)]$ sheets become the main products with some precursors existed (at 6 h, Fig. 2B). When the time is 12 h, the obtained samples are all nanosheets with the size of about 400 nm. All XRD peaks of samples (Fig. 2D(C)) can match with those of reported $Bi_2O_2[BO_2(OH)]$ samples, indicating that the nanosheets are $Bi_2O_2[BO_2(OH)]$ with high purity. The crystal structure of $Bi_2O_2[BO_2(OH)]$ is confirmed to be monoclinic crystal with a = 5.4676(6) Å, b = 14.6643(5) Å, c = 3.9058(1) Å, and β=135.587(6)º (space group: Cm).[14-15] The structures of as-prepared $Bi_2O_2[BO_2(OH)]$ nanosheets were further investigated by TEM and HR-TEM which were given in Fig. S1 of ESI. It can be observed from TEM images, the obtained samples are ultrathin nanosheets with a length of about 400 nm and the lattice fringes reveal the nanosheets to be single-crystals which is shown in Fig. S1B of ESI. The influences of reaction temperature, concentration of PVP have been studied and SEM images and XRD patterns of as-prepared samples are given in Fig. S2 of ESI. $Bi_2O_2[BO_2(OH)]$ nanosheets with adjustable thickness from 60 to 15 nm can be obtained as shown in Fig. 3A-C. In order to understand the growth process of $Bi_2O_2[BO_2(OH)]$ nanosheets, a schematic diagram is given in Fig. 2E. At first step, $Bi(NO_3)_3$ hydrolyzes to be precursor $BiONO_3$ plates. $B(OH)_3$ hydrolyzes to be $[BO_2(OH)]^{2-}$ by adjusting pH value of solution. During hydrothermal process, an ion-exchange reaction happens between $[BO_2(OH)]^{2-}$ and $BiONO_3$ on the surface of precursor to generate $Bi_2O_2[BO_2(OH)]$. Because of the layered crystal structures, the generated $Bi_2O_2[BO_2(OH)]$ grows easily to be sheets. The added PVP can be absorbed on the surface of sheets to restrain the growth along <010> direction, resulting in the formation of ultrathin sheets. More detailed chemical reaction equations in growth process are listed in equations S5-S8 of ESI.

Photocatalytic activities of as-prepared samples were evaluated by the degradation of organic pollution Rhodamine B (RhB) under UV light irradiation. As shown in Fig. 3E, $Bi_2O_2[BO_2(OH)]$ nanosheets with thickness of 15 nm can decompose over 95% RhB in 60 min. With the increase of thickness, the degradation rate of RhB becomes slowly; 89 % and 63 % RhB are decomposed over nanosheets by photocatalysts with thickness of 30 nm and 60 nm, respectively. Only a little RhB is photo-decomposed over $Bi_2O_2[BO_2(OH)]$ particels as photocatalysts. For comparison, the $Bi_2O_2CO_3$ without an internal polarized field in crystal structure was used as photocatalyst and only low 10% RhB is decomposed in 60 min. After five times recycle, the photocatalyst $Bi_2O_2[BO_2(OH)]$ exhibits a better stability in photocatalytic reaction. To understand the main reason for photocatalytic activity, surface areas were measured to be 22.41, 49.54 and 50.14 m^2/g for sample A, B and C, respectively. The optical absorptions of the synthesized $Bi_2O_2[BO_2(OH)]$ samples were measured using a UV-Vis diffuse reflection as shown in Fig. S3 of ESI. E_g of $Bi_2O_2[BO_2(OH)]$ is estimated to be 2.96 eV by the equation $\alpha h\nu = A(h\nu - E_g)^{n/2}$ (where α, ν, E_g and A are the absorption coefficient, the light frequency, the band gap and a constant, respectively). E_{CB} and E_{VB} are evaluated to be 0.32 eV and 3.28 with the calculation equations listed in equations S1-S4, more photocatalysis and band structure details are in Fig. S4-S5 of ESI.

To investigate the influence of electronic structure on photocatalytic activity, the electronic structure of $Bi_2O_2[BO_2(OH)]$ was calculated by the equations (1-2):

$$V_i = \sum_j S_{ij} = \sum_j \exp[(R_0 - R_{ij})/B] \quad (1)$$

In equation (1), R_0 =1.371, B=0.37 are the average bond length of B-O bond and a constant, respectively. And R_{ij} is the actual bond length between i and j, S_{ij} is valence of the bond i-j, V_i is bond valence sum of the cation i.

$$\mu = neR \quad (2)$$

Then we use the Debye equation, equation (2), where μ is the net dipole moment in Debye (10-18 esu cm), n is the total number of electrons, e is the charge on an electron, -4.8×10^{-10} esu, and R is the difference, in cm, between the "centroids" of positive and negative charge.[16]

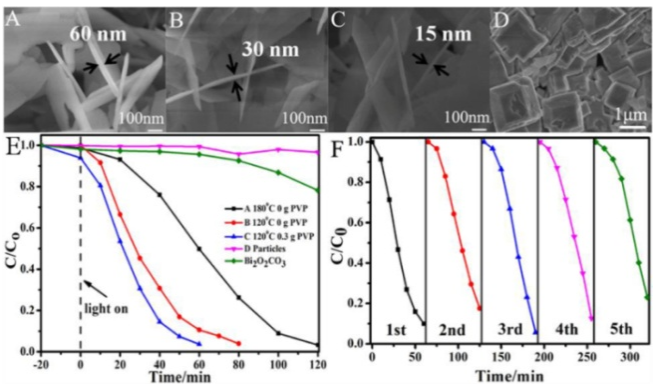

Fig. 3 SEM images of $Bi_2O_2[BO_2(OH)]$ nanosheets (A-C) with different thickness 60 nm (A), 30 nm (B) and 15 nm (C), respectively; particles (D). E) Photocatalytic degradation of RhB over different samples corresponding to (SEM A-D) and $Bi_2O_2CO_3$ as photocatalyst under UV light irradiation. F) Recycle photocatalytic reactions over $Bi_2O_2[BO_2(OH)]$ (SEM C).

The dipole moment of the $BO_2(OH)$ pyramids in unite cell is verified to be 2.41 D by calculation and is along (-2.53140, 0, -3.35829) direction. More detailed data are given in Table S1-S3 of ESI. With the ordered arrangement of $BO_2(OH)$ pyramids in crystal structures, an internal polar field is verified to be existed and its orientation is shown in Fig. 1B. From the crystal structure of $Bi_2O_2[BO_2(OH)]$, we can see the direction of the polar field is in accordance with that of charge transfer in $Bi_2O_2[BO_2(OH)]$. So under the action of internal polar field, the photo-induced electron and hole would transfer along opposite directions, which facilitates the charge separation, resulting in high photocatalytic activity of $Bi_2O_2[BO_2(OH)]$ nanosheets, while $Bi_2O_2[BO_2(OH)]$ irregular particles (Fig. 3D) with block structures don't have layered structure which increases the recombination rate of photo-generated charges, tremendously. As for $Bi_2O_2CO_3$, adjacent Bi_2O_2 layers are related to each other by inversion symmetry and CO_3 pyramids don't have a dipole moment in crystal structure of $Bi_2O_2CO_3$, resulting in no internal polar field in $Bi_2O_2CO_3$.[13]

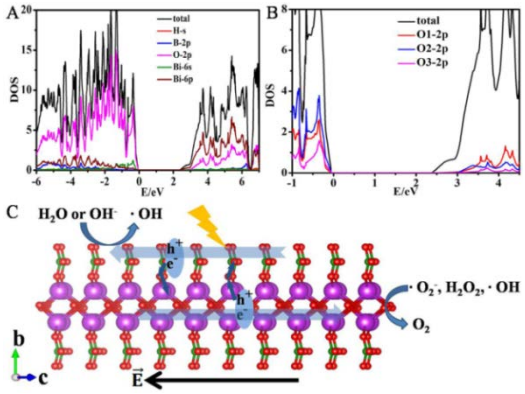

Fig. 4 The total and projected DOS plots calculated for A) $Bi_2O_2[BO_2(OH)]$ and B) different O atoms in $Bi_2O_2[BO_2(OH)]$, C) Schematic illustration showing internal polarized field how to enhance the charge separation and the photocatalytic mechanism of $Bi_2O_2[BO_2(OH)]$.

For understanding the high photocatalytic activity of $Bi_2O_2[BO_2(OH)]$, its electronic band structure was investigated by the density functional calculations, and the density of states (DOS) plots are given in Fig. 4A-B. The VB has strong O 2p contributions, while CB has Bi 6p contributions (Fig. 4A). There are three kinds of oxygen atoms in $Bi_2O_2[BO_2(OH)]$, in which the O1 atoms form the Bi_2O_2 layers, the O2 atoms belong to $BO_2(OH)$ and bridge Bi_2O_2 layers and $BO_2(OH)$ pyramids, and the O3 atoms are the terminal atoms of $BO_2(OH)$ to link H atoms and B atoms (Fig. 1). The VB top has O 2p contributions and O1 O2 atoms have a similar contribution value (Fig. 4B), so the photo-excitations from the VB top to CB generate holes at the O 2p states in all O atoms, especially in O1 and O2. In an approximate way, the CB bottom has Bi 6p primary contributions and O1 2p secondary contributions from Bi_2O_2 layers (Fig. 4B), thus the photo-generated electrons can be gathered in Bi_2O_2 layers and cease at the p-states of the Bi^{3+} sites (Fig. 4C). As is described in Fig. 4, with a polar electric field in crystal structure of $Bi_2O_2[BO_2(OH)]$, photo-generated charges at Bi_2O_2 layers can migrate through the O2 atoms to adjacent $BO_2(OH)$ pyramids, and vice versa. It is noted that the CB bottom has no B states contribution, which suggests that the electrons are mainly generated at Bi_2O_2 layers. So when electrons and holes are separated at $BO_2(OH)$ pyramids, electrons can move to adjacent Bi_2O_2 layers by means of bridging O2 whose contribution to CB is present, while holes can be trapped in –O3H perssads because of their vertical orientation with the direction of internal polar field or maintain at O2. This e-h separation at each $BO_2(OH)$ pyramid will be enhanced by the internal polar field. In a similar manner, the photo-generated holes at Bi_2O_2 layers can move through the bridging O2 to the $BO_2(OH)$ pyramids and eventually be immobilized on the O atoms of $BO_2(OH)$ pyramids, while the photo-generated electrons might end up in the Bi 6p at CB bottom. In general, electrons and holes are gathered at Bi_2O_2 layers and $BO_2(OH)$ pyramids, respectively,[12] separated along *b* axis. Furthermore, the internal polar field promotes their separation along the field direction in *ac* plane (Fig. 4C). Finally, photo-generated electrons are consumed at the edge of $Bi_2O_2[BO_2(OH)]$ nanosheets by reduction reaction, while holes are consumed at the surface by oxidation reaction, which reveals that both these reactions can easily proceed on thinner nanosheets. Even with similar band gap for $Bi_2O_2[BO_2(OH)]$ and $Bi_2O_2CO_3$, their huge differences in photocatalytic activities can further support our conclusion that the existence of internal polar electric field facilitates charge separation resulting in higher photocatalytic efficiency.

Conclusions

In summary, $Bi_2O_2[BO_2(OH)]$ with nanosheet structures was firstly synthesized by using hydrothermal method. With nonzero dipole moment of the $BO_2(OH)$, an internal polar electric field was constructed along the *ac* plane in the crystal structure of $Bi_2O_2[BO_2(OH)]$. The electronic structure of $Bi_2O_2[BO_2(OH)]$ was investigated to indicate that the photo-generated electrons and holes were carried mainly in Bi_2O_2 and $BO_2(OH)$ layers, respectively. The internal polar electric field facilitates the charge separation due to opposite movement of electrons and holes in electric field, resulting in higher photocatalytic efficiency of $Bi_2O_2[BO_2(OH)]$ than that of $Bi_2O_2CO_3$ which has no existence of internal polar electric field. What's more, the layered structure of $Bi_2O_2[BO_2(OH)]$ is favor for the usage of internal polar electric field while irregular $Bi_2O_2[BO_2(OH)]$ particles have a small specific surface area and low charge separation efficiency which makes the internal polar electric field useless. This work provided a further understanding for the construction of internal polar electric field and its promotion of charge separation.

This work was financially supported by a research Grant from the National Basic Research Program of China (the 973 Program; No. 2013CB632401), the National Natural Science Foundation of China (Nos. 21333006, 51321091, 21007031 and 2011374190).

Notes and references

[a] State key lab of crystal materials, Shandong university, Jinan, China, 250100. Email: bbhuang@sdu.edu.cn

[b] School of physics, Shandong university, Jinan, China, 250100. Email: daiy60@sdu.edu.cn

† Electronic Supplementary Information (ESI) available: Experimental details, Figure S1-S5, equation S1-S8, Table S1-S3. See DOI: 10.1039/c000000x/

1 A. Fujishima and K. Honda, *Nature*, 1972, **238**, 37.
2 P. Wang, B. B. Huang, X. Y. Qin, X. Y. Zhang, Y. Dai, J. Y. Wei and M-H. Whangbo, *Angew. Chem. Int. Ed.*, 2008, **47**, 7931.
3 M. L. Guan, C. Xiao, J. Zhang, S. J. Fan, R. An, Q. M. Cheng, J. F. Xie, M. Zhou, B. J. Ye and Y. Xie, *J. Am. Chem. Soc.*, 2013, **135**, 10411.
4 J. P. Wang, B. B. Huang, Z. Y. Wang, P. Wang, H. F. Cheng, Z. K. Zheng, X. Y. Qin, X. Y. Zhang, Y. Dai and M-H. Whangbo, *J. Mater. Chem.*, 2011, **21**, 4562.
5 G. Liu, L. Z. Wang, H. G. Yang, H. M. Cheng and G. Q. Lu, *J. Mater. Chem.*, 2010, **20**, 831.
6 G. Cheng, J. Y. Xiong and F. J. Stadler, *New J. Chem.*, 2013, **37**, 3207.
7 L. Xie, J. Ma and G. Xu, *Mater. Chem. Phys.*, 2008, **110**, 197.
8 G. Tian, Y. Chen, W. Zhou, K. Pan, Y. Dong, C. Tian and H. Fu, *J. Mater. Chem.*, 2010, **20**, 887.
9 R. Buonsanti, V. Grillo, E. Carlino, C. Giannini, F. Gozzo, M. Garcia.-Hernandez, M. A. Garcia, R. Cingolani and P. D. Cozzoli, *J. Am. Chem. Soc.*, 2010, **132**, 2437.
10 L.Pan, J. J. Zou, X. W. Zhang and L. Wang, *J. Am. Chem. Soc.*, 2011, **133**, 10000.
11 M. Teranishi, S. Naya and H. Tada, *J. Am. Chem. Soc.*, 2010, **132**, 7850.
12 S. D. Nguyen, J. Yeon, S. H. Kim and P. S. Halasyamani, *J. Am. Chem. Soc.*, 2011, **133**, 12422.
13 W. J. Wang, B. B. Huang, X. C. Ma, Z. Y. Wang, X. Y. Qin, X. Y. Zhang, Y. Dai and M-H. Whangbo, *Chem. Eur. J.*, 2013, **19**, 14777.
14 R. H. Cong, J. L. Sun, T. Yang, M. R. Li, F. H. Liao, Y. X. Wang and J. H. Lin, *Inorg. Chem.*, 2011, **50**, 5098.
15 H. W. Huang, Y. He, Z. S. Lin, L. Kang and Y. H. Zhang, *J. Phys. Chem. C*, 2013, **117**, 22986.
16 P. A. Maggard, T. S. Nault, C. L. Stern and K. R. Poeppelmeier, *J. Solid State Chem.*, 2003, **175**, 27.

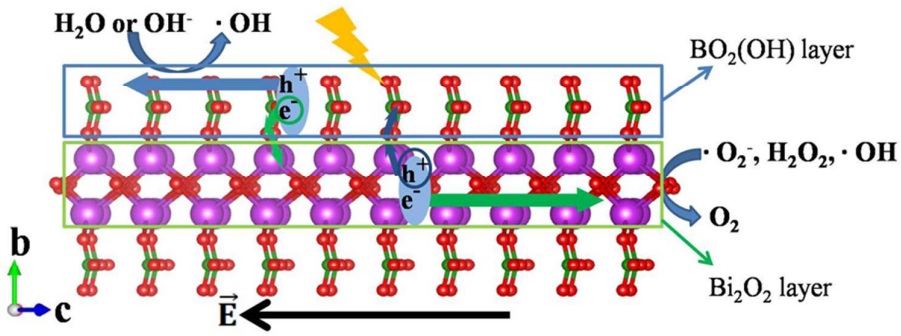

Layered photocatalyst $Bi_2O_2[BO_2(OH)]$ nanosheets efficiently separate photo-generated carriers due to the internal polar electric field, which enhance its photocatalytic activity.